Low-energy tail of the giant dipole resonance in ^{98}Mo and ^{100}Mo deduced from photon-scattering experiments

G. Rusev,[1,*] R. Schwengner,[1] F. Dönau,[1] M. Erhard,[1] E. Grosse,[1,2] A. R. Junghans,[1] K. Kosev,[1] K. D. Schilling,[1] A. Wagner,[1] F. Bečvář,[3] and M. Krtička[3]

[1]*Institut für Strahlenphysik, Forschungszentrum Dresden-Rossendorf, D-01314 Dresden, Germany*

[2]*Institut für Kern- und Teilchenphysik, Technische Universität Dresden, D-01062 Dresden, Germany*

[3]*Faculty of Mathematics and Physics, Charles University, CZ-18000 Prague 8, Czech Republic*

(Received 30 May 2007; published 30 June 2008)

Dipole-strength distributions in the nuclides ^{98}Mo and ^{100}Mo up to the neutron-separation energies have been studied in photon-scattering experiments at the bremsstrahlung facility of the Forschungszentrum Dresden-Rossendorf. To determine the dipole-strength distributions up to the neutron-emission thresholds, statistical methods were developed for the analysis of the measured spectra. The measured spectra of scattered photons were corrected for detector response and atomic background by simulations using the code GEANT3. Simulations of γ-ray cascades were performed to correct the intensities of the transitions to the ground state for feeding from higher-lying levels and to determine their branching ratios. The photoabsorption cross sections obtained for ^{98}Mo and ^{100}Mo from the present (γ, γ') experiments are combined with (γ, n) data from literature, resulting in a photoabsorption cross section covering the range from 4 to about 15 MeV of interest for network calculations in nuclear astrophysics. Novel information about the low-energy tail of the giant dipole resonance and its energy dependence is derived. The photoabsorption cross sections deduced from the present photon-scattering experiments are compared with existing data from neutron capture and ^{3}He-induced reactions.

DOI: 10.1103/PhysRevC.77.064321 PACS number(s): 24.30.Cz, 25.20.Dc, 27.60.+j

I. INTRODUCTION

Among the collective modes of nuclei the electric dipole ($E1$) excitation has the special property that most of its strength is concentrated in the isovector giant dipole resonance (GDR). Macroscopically, this strong resonance is described as a vibration of the charged (proton) matter in the nucleus against the neutral matter (neutrons) [1–3]. It is a long-standing question of nuclear physics to specify how much of the $E1$ strength is still present at energies far below the GDR maximum. Theoretically it has been shown [4] that it is justified to describe the GDR by a Lorentzian also below the particle emission thresholds. Herewith it is important that the contribution of particle emission, i.e., the escape widths, to the total width of the GDR is negligible [5]. Various experimental attempts to determine the low-energy extension of the GDR for heavier nuclei have led to conflicting results. Neutron-capture experiments often have indicated an overshoot of the Lorentzian over the observed $E1$ strength at the low-energy tail of the GDR [6]. On the basis of these data theoretical explanations have been proposed [7] to explain the differences that include the posit of a strong energy dependence of the GDR width. Photon-scattering experiments, however, are in some cases in reasonable agreement with the Lorentzian extrapolation [8,9]. However, in some nuclei extra strength [10] with respect to the smooth Lorentzian was found and denoted as "pygmy dipole resonance" (PDR) [11] in contrast to the GDR. The PDR has experimentally been studied so far in spherical nuclides around $Z, N = 20, 28$, $Z = 50$, $N = 82$, and in the doubly magic ^{208}Pb. An overview about these studies is given in Ref. [12]. Theoretical approaches describe the PDR as caused by an oscillation of excessive neutrons against the symmetric proton-neutron system (see, e.g., Refs. [13–15]). New experimental studies of the behavior of the dipole strength on the tail of the GDR in a wider area of the nuclear chart accounting for properties like nuclear deformation, etc., are needed for a deeper understanding of the PDR.

The measurement of the photoabsorption cross section σ_γ at energies close to the neutron-separation energy is faced with the following problems: Below the neutron threshold σ_γ can be measured via γ rays emitted after photoexcitation. However, the increasing density of nuclear states toward the threshold leads to complex de-excitation patterns that include the de-excitation not only to the ground state (elastic scattering) but also to many intermediate states (inelastic scattering). Hence, the intensities of the transitions to the ground state drop rapidly toward high excitation energies, whereas many branching transitions to intermediate states appear in the low- and medium-energy part of the γ-ray spectrum. Because the assignment of the several hundred transitions observed in a spectrum to certain states is practically impossible, the determination of the dipole-strength distribution at high energies requires an appropriate method to correct it for the corresponding branching ratios and possible feeding from higher-lying states. Above the (γ, n) threshold σ_γ has been measured by detecting neutrons following photoabsorption [16]. Apparently, the absorption cross section closely above the threshold for neutron emission is small and accurate data are difficult to obtain for these energies [17].

In this work we present results of photon-scattering experiments in the energy region from 4 MeV to the neutron-emission thresholds for the molybdenum isotopes with mass

*Present address: Department of Physics, Duke University, Triangle Universities Nuclear Laboratory, Durham, NC 27708, USA.

numbers $A = 98$ and 100, performed at the superconducting electron accelerator ELBE of the Forschungszentrum Dresden-Rossendorf. For the first time photon-scattering spectra are corrected with respect to branching and feeding transitions by applying statistical methods. In this way, we obtain information about the behavior of the photoabsorption cross section in the region closely below the neutron-separation energy and, thus, about the dipole strength on the low-energy tail of the GDR. We propose a parametrization of the low-energy tail of the GDR based on spectroscopic properties of the respective nucleus near its ground state. On this basis an extension of the knowledge on the form of the GDR from stable to exotic nuclei seems possible, which is important for astrophysical applications.

II. EXPERIMENTAL CONSIDERATIONS

A. Photon scattering

In photon scattering from nuclei, an excited level is populated by resonant absorption of a real photon. The level can de-excite to the ground state or to some intermediate levels by γ-ray transitions. The process of photon scattering is also called nuclear resonance fluorescence (NRF) [18,19]. The probability to excite a level with spin J_R from the ground state with spin J_0 is given by the photoabsorption cross section integral I_R over the resonance R:

$$I_R = \int_0^\infty \sigma_\gamma(E)dE = \frac{2J_R+1}{2J_0+1}\left(\frac{\pi\hbar c}{E_R}\right)^2 \Gamma_0, \qquad (1)$$

where E_R is the energy of the populated level with angular momentum J_R, and Γ_0 is the partial width of the transition to the ground state. Because of the low-momentum transfer in photon scattering, mainly levels with spin J_R that satisfy the condition $|J_0 - 1| \leqslant J_R \leqslant J_0 + 1$ are excited.

In the case of nonoverlapping resonances, photon scattering is described to proceed via a compound-nucleus reaction with uncorrelated channels f characterized by the partial widths Γ_f. The photon-scattering cross section $\sigma_{\gamma f}$ representing the process of excitation of a level E_R and de-excitation to a level E_f is expressed as:

$$\sigma_{\gamma f}(E_R) = \sigma_\gamma(E_R)\frac{\Gamma_f}{\Gamma}, \qquad (2)$$

where all partial widths contribute to the total level width $\Gamma = \sum \Gamma_f$. In integral form, Eq. (2) can be written as:

$$I_s = \int_0^\infty \sigma_{\gamma f}(E)dE = \frac{2J_R+1}{2J_0+1}\left(\frac{\pi\hbar c}{E_R}\right)^2 \Gamma_0 \frac{\Gamma_f}{\Gamma}, \qquad (3)$$

where I_s is the scattering cross section integral for the level R and Γ_f is the partial width for a transition from R to a level f. The case $f = 0$ corresponds to elastic scattering, i.e., de-excitation to the ground state. The corresponding elastic-scattering cross section is labeled $\sigma_{\gamma\gamma}$. The determination of Γ_0 from I_s for a level R excited by absorption of a photon from the ground state requires the identification of all transitions de-exciting the level R to calculate the branching ratios Γ_f/Γ [cf. Eq. (3)]. The intensity $I_\gamma(E_\gamma, \theta)$ of a considered transition to the ground state at $E_\gamma = E_R$ measured at an angle θ relative to the incident photon beam is expressed as:

$$I_\gamma(E_\gamma, \theta) = I_s(E_R)\Phi(E_R)\varepsilon(E_\gamma)N_{\text{at}}W(\theta)\frac{\Delta\Omega}{4\pi}, \qquad (4)$$

where $W(\theta)$ is the angular correlation of this transition, $\Delta\Omega$ is the solid angle under which the detector views the sample, $\Phi(E_R)$ is the absolute photon flux at E_R, $\varepsilon(E_\gamma)$ is the absolute full-energy-peak efficiency, and N_{at} the number of atoms in the sample.

In our photon-scattering experiments we used bremsstrahlung produced by deceleration of electrons in a thin metallic foil (radiator) that allows an excitation of many levels in a wide energy range. If the electron energy is high enough above a particular level, the experiments with bremsstrahlung lead to the possibility of the population of a level by a feeding transition from a higher-lying level. Such feeding increases the intensity of the transition to the ground state from the considered resonance R. The intensity of the transition to the ground state becomes a superposition of the rate of elastic scattering and the intensity of the transitions feeding level R. The cross-section integral I_{s+f} deduced for this case can be expressed in a more general form as:

$$\begin{aligned} I_{s+f} &= \int_0^\infty \sigma_{\gamma\gamma}(E)dE + \sum_{i>R}\int_0^\infty \sigma_{\gamma i}(E)\frac{\Gamma_0}{\Gamma}dE \\ &= \frac{2J_R+1}{2J_0+1}\left(\frac{\pi\hbar c}{E_R}\right)^2\frac{\Gamma_0^2}{\Gamma} \\ &\quad + \sum_{i>R}\frac{\Phi(E_i)}{\Phi(E_R)}\frac{2J_i+1}{2J_0+1}\left(\frac{\pi\hbar c}{E_i}\right)^2\Gamma_0^i\frac{\Gamma_R^i}{\Gamma^i}\frac{\Gamma_0}{\Gamma}, \end{aligned} \qquad (5)$$

where summation over $i > R$ means that the energy E_i of a level which feeds the considered resonance R is higher than the energy E_R of this resonance. The quantities Γ^i, Γ_0^i, and Γ_R^i are the total width of the level E_i, the partial width of the transition to the ground state and the partial width of the transition to the level R, respectively. Taking into account the elastic and inelastic photon scattering, the intensity of the transition to the ground state de-exciting the resonance R can be obtained from Eq. (4) by substitution of I_s with the expression given in Eq. (5) using a proper expression for the angular distribution of cascade transitions as discussed below. It is evident that the correct determination of the scattering integral from photon-scattering experiments with bremsstrahlung requires a correction for the intensity of the feeding transitions and for the branching ratio Γ_0/Γ.

The measurement of the angular distribution of the scattered photons γ_2 with respect to the incoming photon beam γ_1, i.e., for the sequence $J_0 \xrightarrow{\gamma_1} J_R \xrightarrow{\gamma_2} J_0$, allows a spin assignment of the excited states. The angular correlation function $W(\theta)$ of the scattered photons for the case of multipolarity $L \leqslant 2$ can be written as:

$$W(\theta) = \sum_{\lambda\text{even}} B_\lambda(\gamma_1)A_\lambda(\gamma_2)P_\lambda(\cos\theta), \qquad (6)$$

where the expansion coefficients A_λ and B_λ are frequently used in the phase convention of Krane and Steffen [20]. The angular dependence is included by the Legendre polynomials

$P_\lambda(\cos\theta)$. The ratios of the transition intensity measured at 90° over the intensity at 127° for the spin sequences of $0 \to 1 \to 0$ and $0 \to 2 \to 0$ have values of 0.73 and 2.28, respectively, according to Eq. (6). The opening angles of 16° and 14° of the detectors at 90° and 127° change these values to 0.74 and 2.18, respectively. This allows an assignment of the multipole order of the scattered radiation and the angular momentum of the excited level E_R.

In the general case, one or more intermediate transitions may occur before the γ-ray of interest is observed. Those intermediate transitions may lead to a redistribution of the population of the substates and may be taken into account by including appropriate coefficients U_λ in Eq. (6). The angular distribution function has the general form [21]:

$$W(\theta) = \sum_{\lambda\ \mathrm{even}} B_\lambda(\gamma_1) U_\lambda(\gamma_1') \cdots U_\lambda(\gamma_{n-1}') A_\lambda(\gamma_2) P_\lambda(\cos\theta), \tag{7}$$

where the expansion coefficients U_λ are:

$$U_\lambda(\gamma) = \frac{U_\lambda(L) + \delta_2^2 U_\lambda(L')}{1+\delta_2^2}, \tag{8}$$

$$U_\lambda(L) = (-1)^{J_i+J_f+\lambda+L}\sqrt{(2J_i+1)(2J_f+1)}\begin{Bmatrix} J_i & J_i & \lambda \\ J_f & J_f & L \end{Bmatrix}. \tag{9}$$

The mixing ratio δ_2 for the observed transition γ_2 is defined by the reduced matrix elements to:

$$\delta_2 = \frac{\langle J_n \| \hat{L}_2' \| J_{n-1} \rangle}{\langle J_n \| \hat{L}_2 \| J_{n-1} \rangle}, \tag{10}$$

where $L_2' = L_2 + 1$.

The predicted value for the ratio $W(90°)/W(127°)$ for the last transition of a cascade of spin sequences $0 \to 1 \to 1 \to 0, 0 \to 1 \to 2 \to 0$ and $0 \to 2 \to 1 \to 0$ is 1.0 and for the sequence $0 \to 2 \to 2 \to 0$ it is 1.14.

B. Dipole strength function

The radiative strength functions characterize the excitation and de-excitation γ-ray transitions in the nucleus. The strength function is defined as the mean reduced transition width, see, e.g., Ref. [11]. In general, two types of strength function are distinguished: (i) the "downward" strength function $\overleftarrow{f}_{XL}(E_\gamma)$ related to deexciting transitions:

$$\overleftarrow{f}_{XL}(E_\gamma) = E_\gamma^{-(2L+1)} \frac{\langle \Gamma_i^{XL}(E_\gamma) \rangle}{D(E_R)}, \tag{11}$$

and (ii) the "upward" strength function $\vec{f}_{XL}(E_\gamma)$ related to the excitation of the levels from the ground state, i.e., depending only on the Γ_0 widths:

$$\vec{f}_{XL}(E_\gamma) = E_\gamma^{-(2L+1)} \frac{\langle \Gamma_0^{XL}(E_\gamma) \rangle}{D(E_R)}, \tag{12}$$

where $\Gamma_i^{XL}(E_\gamma)$ is the partial width for a transition to level i ($i = 0$ is the ground state) of type X, multipolarity L, and energy E_γ. D is the average spacing of the levels near the excited resonance E_R. In the case of photon scattering, radiation with multipolarity $L > 1$ contributes only weakly to the absorption of photons, such that $\vec{f}_{XL}(E_\gamma) = \vec{f}_{M1}(E_\gamma) + \vec{f}_{E1}(E_\gamma) + E_\gamma^2 \vec{f}_{M2}(E_\gamma) + E_\gamma^2 \vec{f}_{E2}(E_\gamma) + \ldots \approx \vec{f}_1(E_\gamma)$. According to Eq. (1), the "upward" dipole-strength function can be related to the average photoabsorption cross section $\langle \sigma_\gamma \rangle$:

$$\vec{f}_1(E_\gamma) = \frac{2J_0+1}{2J_R+1} \frac{\langle \sigma_\gamma(E_R) \rangle}{(\pi\hbar c)^2 E_R}. \tag{13}$$

Note that for the excitation $E_R = E_\gamma$. The dipole-strength function $\vec{f}_1(E_\gamma)$ depends on the superposition of the cross section of the giant dipole $E1$ resonance and $M1$ resonances. It is reasonably well established for many heavy and medium mass nuclei in the region of the GDR by (γ, n) studies, which often have covered the region starting directly above the neutron threshold S_n. The contribution of the $M1$ excitations to $\vec{f}_1(E_\gamma)$ is typically by one order of magnitude smaller than the $E1$ contribution and it is frequently not taken into account [22–24]. From previous experiments information about $M1$ strengths was obtained from discrete transitions [25] in reasonable agreement with calculations within a quasiparticle random-phase approximation (QRPA) in a deformed basis, which confirm the relative weakness of $M1$ strength [25].

The "downward" strength function $\overleftarrow{f}_1(E_\gamma)$ below S_n is derived from the γ rays de-exciting levels populated in capture of thermal neutrons or in reactions with heavy ions. Assuming the validity of the Brink-Axel hypothesis [8], which was tested experimentally for example in a dedicated (γ, p) study [26], one postulates equivalence of the "downward" and "upward" strength functions. This allows the determination of the photoabsorption cross section in an indirect way from observed γ rays from levels excited otherwise than by the absorption of photons.

Strength functions have been deduced so far from (^{3}He,^{3}He$'\gamma$) and (^{3}He,$\alpha\gamma$) reactions in the energy range between about 1 and 7 MeV [27] and from intensities of primary transitions from (n, γ) reactions [28]. Photon-scattering experiments with tagged photons were performed for ^{92}Mo and ^{96}Mo in the region of the GDR [29]. In this work we present a method for a determination of the photoabsorption cross section and the related strength function $\vec{f}_1(E_\gamma)$ below the neutron-separation energy on the basis of photon-scattering experiments.

C. Simulations of γ-ray cascades

In photon-scattering experiments, a fraction of the observed γ rays results from transitions to the ground state. The ratio of the intensities of the transitions to the ground state to that of branching transitions decreases with increasing excitation energy because of the large number of intermediate levels available from the de-excitation of the initial one. The determination of the branching transitions becomes increasingly difficult at high (> 4 MeV) energy. Therefore, we apply statistical methods to estimate the intensities of the branching transitions relative to the transitions to the ground state [30].

We developed a Monte Carlo code for the simulation of γ-ray cascades analogously to the strategy of the code DICEBOX [31]. The nucleus is modeled by a nuclear realization consisting of (i) a level scheme including levels with spin $J = 0$, 1, and 2 and (ii) an assignment of partial decay widths for $E1$, $M1$, or $E2$ transition depopulating every level.

The level density is calculated according to the back-shifted Fermi gas (BSFG) model. The level-density parameter a and the back-shift energy E_1 were taken from the systematics presented in Ref. [32]. We used parameters for ^{98}Mo of $a = 12.28(17)$ MeV^{-1} and $E_1 = 0.75(6)$ MeV and for ^{100}Mo of $a = 13.12(19)$ MeV^{-1} and $E_1 = 0.66(6)$ MeV. Every level scheme was created for values of the parameters within the given uncertainties. The densities of levels with positive parity and with negative parity are assumed to be equal according to Ref. [33]. The Wigner distribution (see, e.g., Ref. [34]) is used for the fluctuation of the nearest-neighbor spacings of levels with the same spin to include the effect of level repulsion. Optionally in the program, the level density can be calculated in the constant temperature (CT) approximation.

A priori strength functions for $E1$, $M1$, and $E2$ transitions are used to calculate the average decay widths of the levels. The strength function for the $E1$ transitions is derived from a parametrization of the giant dipole resonance for triaxially deformed nuclei as discussed in Sec. IV. It was shown in experiments with polarized photon beams on closed-shell nuclei that the prominent transitions below the neutron-separation energy are $E1$ transitions, see e.g., Refs. [35,36]. The strength function for $M1$ transitions was taken from QRPA calculations in a deformed basis for the stable even-mass Mo isotopes [25]. The QRPA calculations reproduce the scissors mode and the spin-flip $M1$ resonance in the Mo isotopes but with a strength smaller than the measured one. We normalized the calculated $M1$ strength to the measured one in the excitation range up to 4 MeV. Data from two-step cascades following thermal neutron capture in ^{162}Dy [37,38] show that the scissors mode and the $M1$ spin-flip resonance are built not only on the ground state but also on excited states, including the levels in the quasicontinuum in accordance with the Brink hypothesis. The strength function for $E2$ transitions was taken from a global parametrization of the $E2$ isoscalar giant resonance provided by RIPL-2 [39]. The Porter-Thomas distribution [40] is used for the fluctuations of the partial decay widths of the levels around the average obtained from the strength function.

The simulation of the γ-ray cascades starts with the excitation of a level with spin $J = 1$ according to the photoabsorption cross section [cf. Eq. (1)]. The de-excitation of the level is governed by the branching ratios for decay to the ground state or to any intermediate level calculated from the partial decay widths $B_f = \Gamma_f / \Gamma$. If the decay is not to the ground state, then the populated intermediate level is considered an excited level and a new transition is performed until the ground state is reached. The code provides energy, spin, and parity of the initial and the final state as well as the multipole order of the transition. The angular distribution of the transitions is calculated according to Eq. (7) which includes the general case of cascade transitions. Because one nuclear realization does not represent completely the properties of the nucleus, but is only a sample, the cascade simulations have to run for many nuclear realizations. The simulations presented in this article were performed for 1000 nuclear realizations.

We apply the statistical methods also for the low-energy part of the level scheme instead of using experimentally known low-lying levels in ^{98}Mo and ^{100}Mo because this would require the knowledge of the partial decay widths of all transitions populating these fixed levels. As shown in Sec. III the level density predicted by the BSFG model at low excitation energy is consistent with experimental values deduced from our previous experiments [25]. Taking into account that there is no excited level below 735 keV in ^{98}Mo and 536 keV in ^{100}Mo one expects no feeding intensity in the energy range from the energy E_x of an excited state down to the maximum energy of an inelastic transition, i.e., E_x minus the energy of the first excited state. This is not exactly fulfilled in the simulations described in Sec. III. However, it will be shown that the small level density used at low excitation energy leads to negligibly small feeding intensity in that energy range.

III. EXPERIMENTAL RESULTS

The present article reports on photon-scattering experiments for the nuclei ^{98}Mo and ^{100}Mo carried out at the bremsstrahlung facility at the superconducting electron accelerator ELBE of the Forschungszentrum Dresden-Rossendorf. Bremsstrahlung was produced by electrons hitting a 7μm (3.4 mg/cm^2) thick Nb radiator. A narrow photon beam is formed by an Al collimator with a length of 2.6 m and an opening angle of 5 mrad. An absorber made of a 10-cm-long Al cylinder between the radiator and the collimator attenuates the intense low-energy part of the bremsstrahlung spectrum. The photon beam irradiates the target shaped as a disk with a diameter of 2 cm. For background reduction, the target was placed in an evacuated polyethylene tube and the photon beam was absorbed in a well-shielded photon-beam dump after passing the target. The photons scattered from the target were registered in four high-purity Ge detectors (HPGe) with an efficiency of 100% relative to a 3 × 3 in. NaI detector. To determine the multipole order of the scattered γ rays two of the detectors were located at 127° and the other two at 90° with respect to the photon beam at distances of 32 and 28 cm to the target, respectively. The low-energy photons are suppressed by lead absorbers with a thickness of 0.8 and 1.3 cm at the two given angles, respectively, combined with 0.3-cm-thick copper absorbers. The HPGe detectors are equipped with 3-cm-thick escape-suppression shields made of bismuth orthogermanate (BGO) scintillation detectors. The detector resolution is about 5.0 and 7.9 keV at γ-ray energies of 5 and 9 MeV, respectively. The electron energy is determined from spectra of protons measured during the photodisintegration of deuterium when irradiating a deuterated polyethylene film. This technique and further details of the bremsstrahlung facility at the ELBE accelerator are described in Refs. [41,42].

We performed measurements on ^{98}Mo and ^{100}Mo at an electron energy of $E_e^{\mathrm{kin}} = 13.2(1)$ MeV. Because we will study the whole chain of stable even-mass Mo isotopes under identical conditions, this energy was chosen such that it exceeds the highest neutron-separation energy in the isotopic

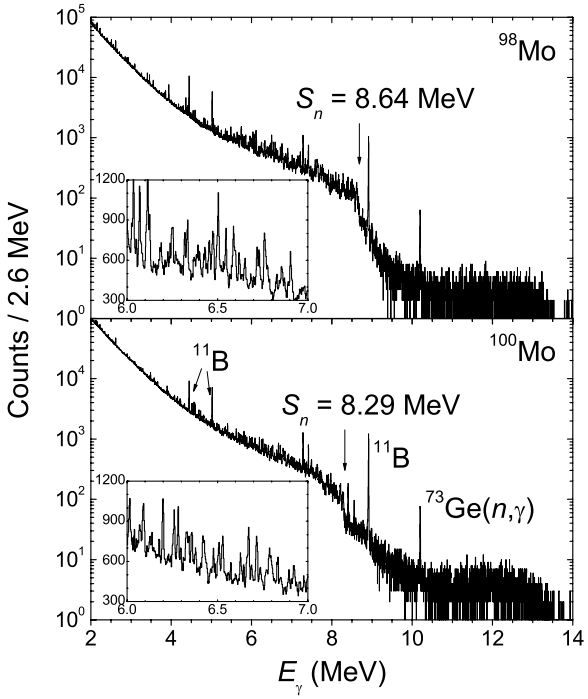

FIG. 1. Spectra of photons scattered from ^{98}Mo and ^{100}Mo at 127° relative to the incident beam. The measurements were performed at identical experimental conditions and an electron-beam energy of 13.2 MeV. Part of the spectra in the range between 6 and 7 MeV are shown in the insets. The neutron-separation energies are indicated with vertical arrows. Strongest peaks from the calibration standard are labeled with ^{11}B.

chain, namely that of ^{92}Mo, $S_n = 12.7$ MeV, by half an MeV to provide a high flux up to S_n. Samples of elementary ^{98}Mo and ^{100}Mo isotopically enriched to 98.55% and 99.27% with masses of 2952.5(1) mg and 2916.8(1) mg, respectively, were used as targets and combined with a 339.5(1) mg sample of ^{11}B enriched to 99.52%. Spectra of photons scattered at 127° from ^{98}Mo and ^{100}Mo measured for 64 h each are presented in Fig. 1. To identify and subtract transitions in the neighboring nuclei produced via (γ, n) reaction additional measurements at $E_e^{\mathrm{kin}} = 8.4(1)$ MeV and $E_e^{\mathrm{kin}} = 7.8(1)$ MeV were performed on ^{98}Mo and ^{100}Mo for 114 and 80 h, respectively.

Simulations for the detector response were performed using the code GEANT3 [43]. The geometry implemented in the simulations includes all elements of the real experimental setup like a beam tube, Pb collimators, Pb and Cu absorbers, HPGe and BGO detectors, and the surrounding passive Pb shield. Examples of simulated detector-response spectra for $E_\gamma = 4$, 7, and 10 MeV are shown in Fig. 2. A comparison of the raw spectrum of ^{100}Mo with the spectrum after detector-response correction is given in Fig. 3. A comparison of the results for the ratio of the full-energy peak to the single-escape peak (FE-to-SE ratio) obtained from simulations and from measurements of the photon-scattering from ^{11}B [44], ^{16}O [45], and ^{28}Si [46] is shown in the inset in Fig. 3.

The full-energy-peak efficiency is obtained using the above detector-response simulations. A comparison of the simulated absolute efficiency with results of measurements with

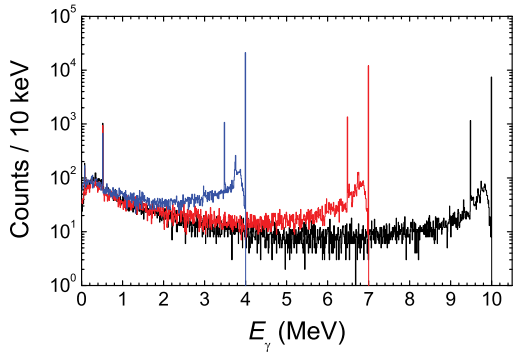

FIG. 2. (Color online) Simulated detector-response spectra for 10^8 monoenergetic γ rays with energies of 4 MeV (blue), 7 MeV (red), and 10 MeV (black) emitted isotropically from the target position. The simulations were performed for one of the HPGe detectors at 127°, including the BGO escape-suppression shield, the beam tube, the Cu and Pb absorbers, and the passive Pb shield and collimator.

calibrated sources ^{22}Na, ^{60}Co, ^{133}Ba, and ^{137}Cs is presented in Fig. 4. Because not all details of the geometry of the HPGe crystal and the surrounding elements of the detector can be exactly defined in GEANT3 the simulated absolute efficiency differs by a few percentages from the one measured with the calibrated sources. We adjusted the result of the simulations to the efficiency deduced from measurements with the calibrated sources. The relative uncertainty of the normalization coefficient is 1.8%. To check the shape of the simulated curve at higher energies, we compare it with the results for the relative efficiency from a ^{56}Co source in Fig. 4. For a check at even higher energies above $E_\gamma = 3.5$ MeV we determined the relative efficiency from the intensities of γ

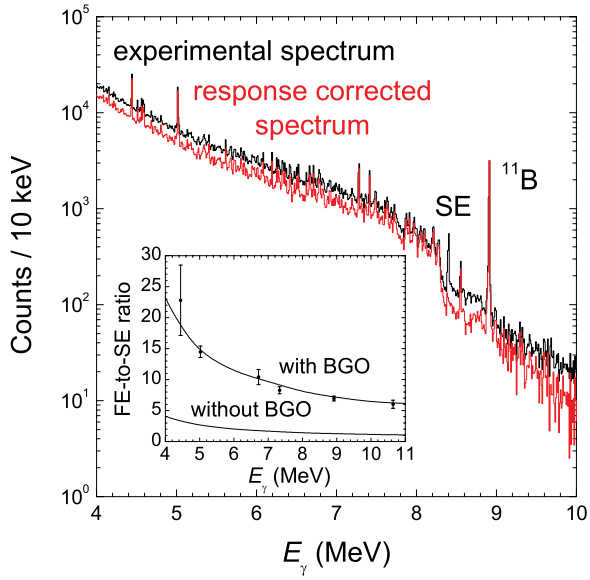

FIG. 3. (Color online) Raw spectrum of photons scattered from ^{100}Mo at 127° in the experiment at $E_e^{\mathrm{kin}} = 13.2$ MeV (upper black) compared with the result of the correction for detector response (lower red). A comparison of the measured ratio of the full-energy peak to the single-escape peak (circles) with results from GEANT3 simulations (solid line) is shown in the inset.

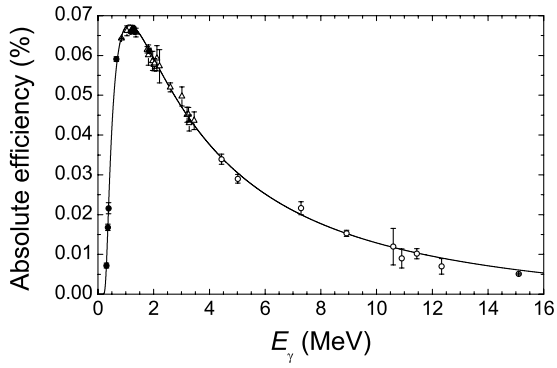

FIG. 4. Absolute full-energy-peak efficiency of the two HPGe detectors placed at 127° measured with calibrated sources ^{22}Na, ^{60}Co, ^{133}Ba, and ^{137}Cs (filled circles) and simulated with GEANT3 (solid line). The relative efficiency deduced from a ^{56}Co source (open triangles) and from the transitions in ^{11}B [44], ^{12}C [44], and ^{28}Si [46] in photon-scattering experiments (open circles) is compared with the simulated one.

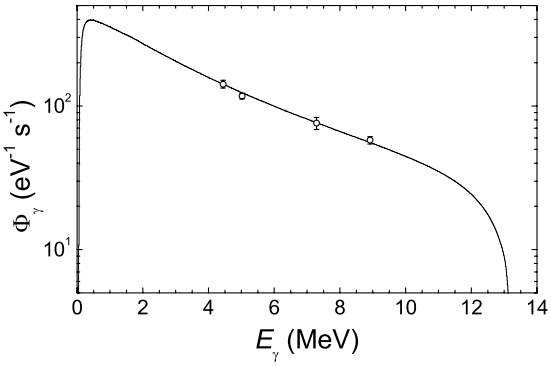

FIG. 5. Photon flux in the ^{100}Mo experiment at $E_e^{\mathrm{kin}} = 13.2$ MeV deduced from the transitions in ^{11}B (data points) compared with the approximation for the bremsstrahlung spectrum according to Ref. [47, 48] (solid line). The calculated curve is corrected for the absorption in the Al hardener and normalized to the photon flux deduced from the 4.445 MeV transition in ^{11}B.

rays scattered from a combined target ^{11}B−$^{\mathrm{nat}}$C−$^{\mathrm{nat}}$Si in 15 different photon-scattering experiments at various electron-beam energies from 9 to 16 MeV. This was done according to Eq. (4) by using the known scattering cross-section integrals of the states in ^{11}B, ^{12}C, and ^{28}Si in connection with fluxes calculated according to Refs. [47,48] (cf. Fig. 5).

Because GEANT3 does not simulate correctly the bremsstrahlung spectrum in the energy range of our experiments [49] we calculated the spectrum from the approximation in Refs. [47,48] for a thin radiator and multiplied the result with the simulated absorption in the Al hardener. The absolute photon flux was derived from the transitions with known cross-section integrals in ^{11}B according to Eq. (4). Properties of the ^{11}B transitions, taken from Ref. [44], are presented in Table I. The values of the mixing ratio δ were taken from Refs. [50,51] and used in the phase convention of Krane and Steffen. The calculated photon flux, normalized to that deduced from ^{11}B, is presented in Fig. 5. The relative uncertainty of the normalization coefficient is 5%. For the two highest states feeding from higher levels can be excluded due to their small energy separation to the particle-emission threshold. The first two states were corrected for feeding according to Eq. (5). The good agreement between the photon flux derived using the simulated efficiency with the calculation for the bremsstrahlung spectrum is a validity test of the simulations.

TABLE I. Properties of transitions in ^{11}B taken from Ref. [44].

E_x[a] (keV)	Γ_0[b] (eV)	B_0[c] (%)	I_s[d] (eVb)	δ[e]	ΠL[f]
4444.9(5)	0.56(2)	100	164(6)	+0.19(3)	$M1/E2$
5020.3(3)	1.68(6)	85.6(6)	219(8)	−0.03(5)	$M1$
7285.5(4)	1.00(7)	87(2)	95(7)	0	$E1$
8920(2)	4.2(2)	95(1)	286(14)	−0.11(4)	$M1/E2$

[a]Level energy.
[b]Partial level width of the ground state.
[c]Branching ratio of the transition to the ground state.
[d]Cross section integral.
[e]Mixing ratio of the transition to the ground state in the phase convention of Krane and Steffen.
[f]Multipolarity of the transition to the ground state.

A. Dipole strength observed in resolved peaks

The spectra of ^{98}Mo and ^{100}Mo (cf. Fig. 1) are characterized by fragmented weak de-excitations. The number of transitions assigned to ^{98}Mo and ^{100}Mo is 485 and 499, respectively. Transitions that do not belong to the investigated Mo isotopes were identified by comparison with spectra measured at electron-beam energy lower than the neutron-separation energy and the information from literature [52,53]. It was found that de-excitations in ^{97}Mo and ^{99}Mo populated in ^{98}Mo and ^{100}Mo, respectively, via the (γ, n) reaction are located in the low-energy part of the spectrum below 4 MeV. The neutrons produced in the target material are thermalized via elastic and inelastic scattering in the experimental hall. Peaks due to γ rays from capture of the thermalized neutrons in the HPGe crystal or the surrounding materials are also observed in the measured spectra. Peaks from ^{A}Ge$(n,\gamma)^{A+1}$Ge, ^{27}Al$(n,\gamma)^{28}$Al, ^{28}Si$(n,\gamma)^{29}$Si, ^{56}Fe$(n,\gamma)^{57}$Fe, and ^{63}Cu$(n,\gamma)^{64}$Cu reactions could be clearly identified and easily subtracted as can been seen by comparison with the corresponding low-energy measurement. A spectrum of neutron-capture induced background is presented in Fig. 6. The measurement was carried out with a ^{244}Cm source combined with ^{13}C producing neutrons via the reaction ^{13}C$(\alpha, n)^{16}$O. The source was placed in a 10 cm thick Pb housing far away from the HPGe detectors to suppress the high-energy γ rays from ^{16}O. The emitted neutrons are thermalized by scattering in the experimental hall and captured in the HPGe crystal or in the surrounding materials. The strongest peaks in the measured γ-ray spectrum in Fig. 6 are labeled with the respective reaction.

Detection limits were determined from the spectra measured at 127° to prove that a peak can be accepted as a transition. The limit, corresponding to 2σ, for the smallest area of a peak P considered as a transition is estimated from

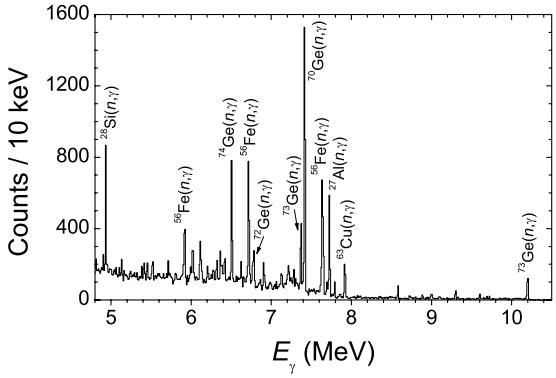

FIG. 6. Spectrum of γ rays following capture of thermal neutrons. The spectrum includes all HPGe detectors. The neutrons produced from ^{13}C$(\alpha, n)^{16}$O reaction in a combined ^{244}Cm/^{13}C source are thermalized by scattering in the experimental hall. The γ rays from the source were suppressed by a 10-cm-thick Pb housing. The strongest peaks in the spectrum are labeled with the respective reaction.

the background in the spectrum according to the relation [54]:

$$P = 1.65\sqrt{2B}. \tag{14}$$

B is the integral over the background of a length of 2σ, where σ is the typical dispersion of a Gaussian fit of the peaks at the same energy. The normalized cross-section integrals $I_{s+f}/3(\pi\hbar c/E_\gamma)^2$ are compared with the detection limits corresponding to 95% confidence limits (2σ) in Fig. 7. A

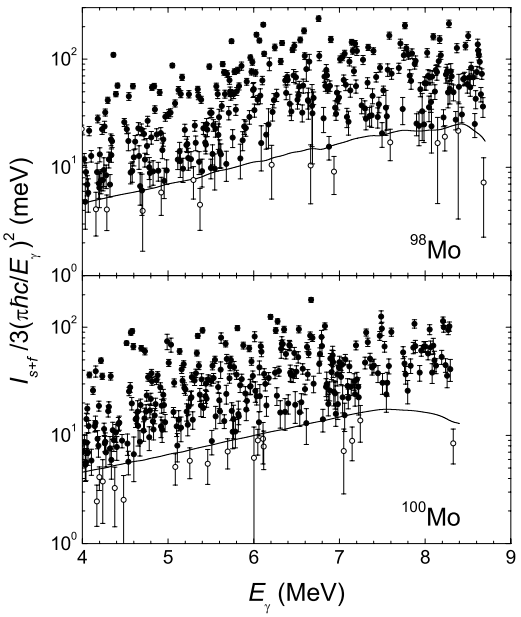

FIG. 7. Comparison of the normalized cross section integrals $I_{s+f}/3(\pi\hbar c/E_\gamma)^2$ for observed transitions, not corrected for feeding and branching transitions, deduced from the experiments on ^{98}Mo and ^{100}Mo (filled circles) at $E_e^{\rm kin} = 13.2$ MeV under the assumption that all transitions are transitions to the ground state, with the detection limits (solid lines). The points marked with open circles are considered being below the detection limits corresponding to 2σ(95% confidence interval).

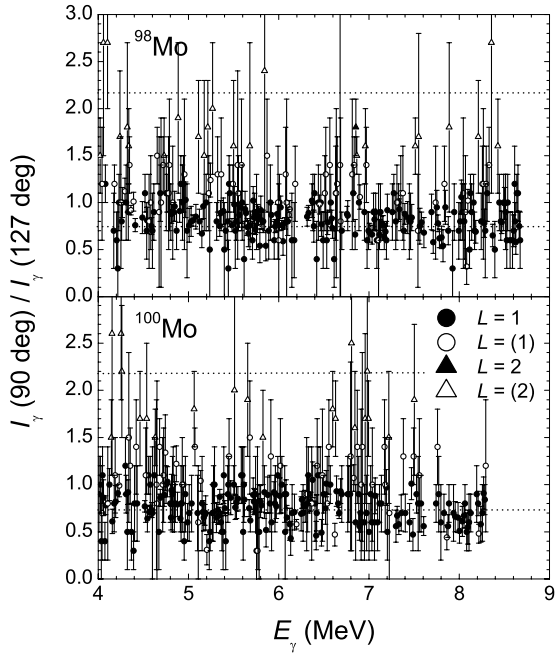

FIG. 8. Ratio of γ-ray intensities at 90° and 127° determined from the experiments at $E_e^{\rm kin} = 13.2$ MeV compared with the predicted values for dipole and quadrupole transitions of 0.74 and 2.18, respectively. The data shown with filled circles are assumed to be dipole transitions.

list of the transitions assigned to ^{98}Mo and ^{100}Mo is given in Ref. [30].

The multipole order of the observed transitions was obtained by comparing the ratios of the γ-ray intensities measured at 90° and 127° with the expected values of 0.74 and 2.22 for dipole and quadrupole radiation, respectively. An assignment of the multipole order of the transition was made if one of the expected values was within two standard deviations of the measured value for the ratio $I_\gamma(E_\gamma, 90°)/I_\gamma(E_\gamma, 127°)$ and the other expected value was excluded by at least three standard deviations. If one of the two criteria was violated, the spin was assigned tentatively. The results for the ratio $I_\gamma(E_\gamma, 90°)/I_\gamma(E_\gamma, 127°)$ are presented in Fig. 8. The comparison with the predicted values for dipole and quadrupole transitions shows that most of the transitions have dipole character.

The density of the observed peaks is compared with predictions of the BSFG and CT models in Fig. 9. The experimental level density stays constant, which reflects the limited detector resolution and the detection limits. The discrepancy to the level density predicted by the models suggests that there are many levels de-excited by weak transitions that are not resolved or not detected. Indeed, the comparison of the experimental spectrum with a simulated atomic background discussed in the next section reveals that there are many weak unresolved transitions that form a continuum in the experimental spectrum.

The feeding intensities of the low-lying levels in ^{98}Mo and ^{100}Mo can be obtained from a comparison of the cross-section integrals deduced at different electron-beam energies. Ratios

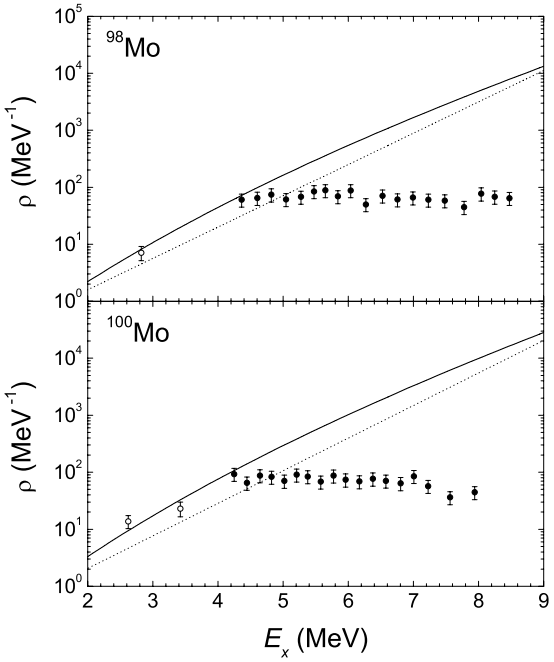

FIG. 9. Density of the transitions assigned to ^{98}Mo and ^{100}Mo (filled circles) compared with the density of levels with $J = 1$ [25] (open circles) and the level density calculated according the back-shifted Fermi gas model (solid lines) and the constant temperature approximation (dotted lines).

of I_s obtained from the measurements at $E_e^{\text{kin}} = 13.2$ MeV and at $E_e^{\text{kin}} = 3.8$ MeV [25] are shown in the top panel of Fig. 10. Some of these levels are fed with intensities exceeding the true elastic-scattering cross-section integrals by factors of more than 10. We performed cascade simulations to investigate the influence of the feeding on the results for I_s from the experiments at $E_e^{\text{kin}} = 13.2$ MeV. The photon flux as taken from Fig. 5 was implemented in the simulations to obtain the correct feeding intensity from the high-lying levels. Ratios of the population of given levels due to photoabsorption and feeding versus the population of these levels by photoabsorption only were calculated that result in I_{s+f}/I_s. Ratios I_{s+f}/I_s averaged over 0.5 MeV are given in the bottom panel of Fig. 10 for excitation energies up to 8 MeV. The results of the cascade simulations show that above about 6 MeV the influence of feeding to the cross section integrals is negligible. This finding is consistent with that found for ^{88}Sr [35]. The calculated ratios I_{s+f}/I_s show a general trend similar to that of the experimental values for individual states, i.e., they reach values up to about 10 at excitation energies around 2 MeV and decrease to values of about two close two 4 MeV. However, the ratios for some of the individual states exceed the average trend. The reason for that may be that transition probabilities between discrete states are determined by their structure. Hence, the structure of specific states may cause stronger feeding by high-lying states than in average. The simulated values, however, do not contain such effects and hence do not reproduce individual values for discrete states, but instead an average behavior for the considered energy bins.

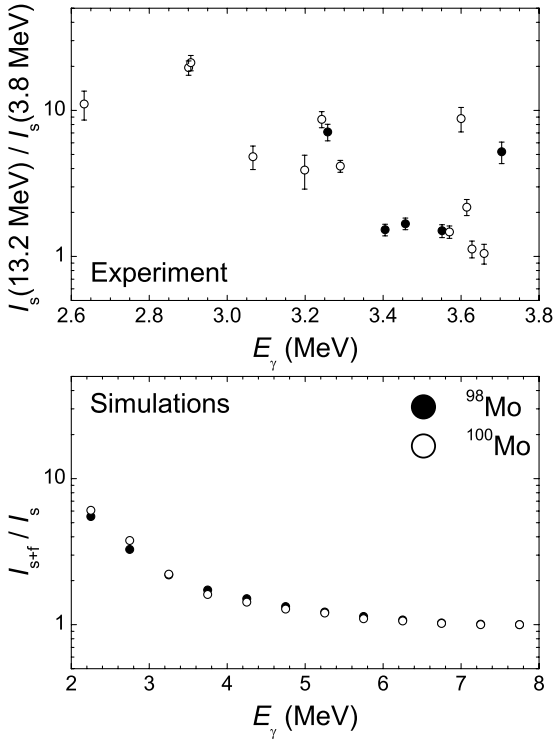

FIG. 10. (Top panel) Ratio of cross-section integrals for low-lying $J = 1$ levels in ^{98}Mo and ^{100}Mo obtained from the experiments at $E_e^{\text{kin}} = 13.2$ MeV and at $E_e^{\text{kin}} = 3.8$ MeV [25]. (Bottom panel) Ratios averaged over 0.5 MeV of intensities resulting from population of levels in ^{98}Mo and ^{100}Mo by photoabsorption as well as feeding versus intensities resulting from the population by photoabsorption only as obtained from cascade simulations using the photon flux shown in Fig. 5.

B. Determination of non-nuclear background radiation

The high level density and the Porter-Thomas fluctuations of the decay widths cause many weak transitions that cannot be observed as resolved peaks. In addition, every level can decay to many intermediate levels via weak transitions. Therefore not all the intensity is carried by observed peaks. Many of the transitions are so weak that their superposition is observed as a quasicontinuum. The intensity "hidden" in the continuum part of the spectrum can be estimated from a comparison of spectra of γ rays scattered from different isotopes. The spectra measured at 127° in the photon-scattering experiments on ^{98}Mo and ^{100}Mo at $E_e^{\text{kin}} = 13.2$ MeV are compared in Fig. 11(a). The spectra are corrected for the natural background; for the neutron-induced background by subtraction of the spectrum shown in Fig. 6 normalized to the area of the peak at 10.2 MeV, which is not contaminated by peaks of ^{11}B and ^{98,100}Mo; and for the detector response. In addition the spectra are corrected for the full-energy peak efficiency (cf. Fig. 4), photon flux (cf. Fig. 5), area density of the target atoms, and the measuring time. The intensity of the peaks of ^{11}B are subtracted from the experimental spectra. The two spectra are characterized by a sudden decrease of intensity at the neutron-separation energy caused by the starting dominance of neutron emission. Above S_n the spectrum contains almost only background from atomic processes, i.e., counts in the

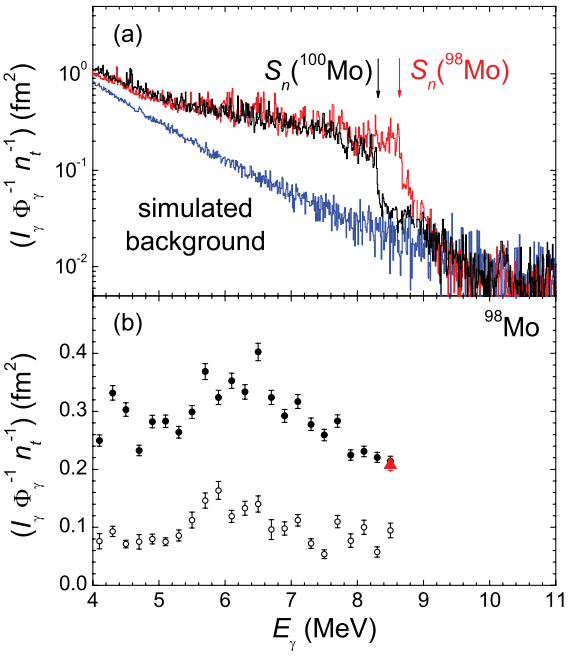

FIG. 11. (Color online) Comparison of the experimental spectra (a) from ^{98}Mo (red) and ^{100}Mo (black) measured at $E_e^{\mathrm{kin}} = 13.2$ MeV corrected for the full-energy peak efficiency, the photon flux Φ_γ, the area density of the target n_t, and the measuring time, with a simulation for the atomic background (blue). The intensities of the peaks from ^{11}B and neutron-capture induced background are subtracted from the experimental spectra. (b) Dipole strength in ^{98}Mo deduced from the resolved peaks (open circles), from subtraction of the background taken from the ^{100}Mo spectrum (red triangle at 8.5 MeV), and from the quasicontinuum (filled circles) after subtraction of the simulated background.

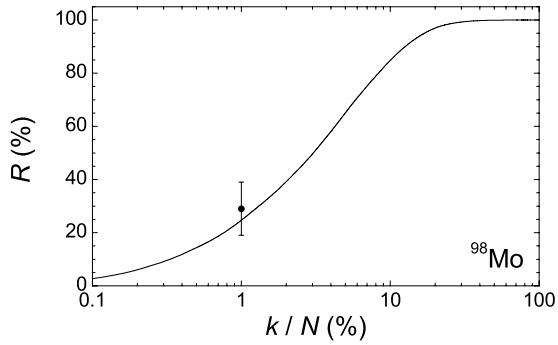

FIG. 12. Ratio of the accumulated elastic-scattering integrals of the k levels with $J = 1$ and with the largest I_s in ^{98}Mo to the superposition of the elastic-scattering integrals for all N levels with $J = 1$ in the scheme of ^{98}Mo up to the neutron-separation energy. The ratio is plotted versus the fraction k/N of the number of considered levels to the total number of levels with $J = 1$. The dependence obtained from the created nuclear realizations of ^{98}Mo (solid line) is in good agreement with the value derived for observed peaks (cf. Figs. 9 and 11).

spectrum that do not result from de-excitations of nuclear levels. Note that the atomic background depends on the amount of the target material. Therefore the experiments on ^{98}Mo and ^{100}Mo were carried out for nearly identical targets with a difference in mass of only about 1%. According to the different neutron-separation energies in ^{98}Mo ($S_n = 8.64$ MeV) and ^{100}Mo ($S_n = 8.29$ MeV) one finds a range between 8.3 and 8.6 MeV in the spectrum of ^{98}Mo for which the atomic background can be taken from the spectrum of ^{100}Mo. The residuum above the spectrum of ^{100}Mo represents the intensity of the γ rays in ^{98}Mo. The intensity in the considered energy range is compared with the intensity deduced from the identified peaks in Fig. 11(b). The ratio of the strength deduced from the experimental spectrum after subtraction of the atomic background to the strength of the resolved peaks at $E_\gamma = 8.5$ MeV is about 3, which means that only about 30% of the strength is located in identified peaks.

Considering Fig. 9, it is visible that the density of the identified peaks in ^{98}Mo at 8.5 MeV is about 1% of the density of levels with spin $J = 1$ predicted by the BSFG model. It is rather surprising that such a small number of levels can carry about 30% of the dipole strength. Note that the transitions close to the neutron-separation energy are transitions to the ground state because the contribution of branching transitions with an energy $E_\gamma \approx 8.5$ MeV de-exciting levels above S_n is negligible. To investigate whether such a small fraction of resolved peaks may be responsible for a large intensity we analyzed the partial widths assigned to the levels of ^{98}Mo in the cascade simulations. The elastic-scattering cross-section integrals for all levels with spin $J = 1$ and energy 8.3 MeV $\leqslant E_x \leqslant 8.6$ MeV were calculated according to Eq. (3) and the levels were counted starting with the largest I_s. The ratio $R = \sum_{i=1}^{k} I_s^i / \sum_{i=1}^{N} I_s^i$ of the summed elastic-scattering cross-section integrals of the first strongest levels k to the summed elastic-scattering cross-section integrals of all $J = 1$ levels in the considered energy range is presented in Fig. 12 versus the ratio k/N. It is evident that about 30% of the intensity is carried by about 1% of the most intense γ-ray transitions only.

It is important to extend the estimate of the atomic background in the measured spectrum to lower energies to determine the total strength in the nucleus. For that purpose we performed GEANT3 simulations of the non-nuclear processes in the target leading to background in the measured spectra. The bremsstrahlung produced in the target by the electrons from Compton scattering and by the electrons and the positrons from the pair creation processes is responsible for the atomic background extending to high energies. As mentioned above, GEANT3 does not reproduce correctly the bremsstrahlung spectrum for energies below 20 MeV. Therefore we exchanged the routine for the calculation of the bremsstrahlung spectrum with one based on the approximation given in Ref. [55].

The simulated atomic background is compared with the spectra of ^{98}Mo and ^{100}Mo in Fig. 11(a). The comparison of simulated quantities with measured ones in Figs. 3 and 4 and the comparison of a simulated with a measured spectrum for ^{12}C given in Ref. [35] show a good agreement and prove that the simulations of the atomic background are correct. Coherent scattering of photons from the nucleus like nuclear Thomson scattering and Delbrück scattering is not included in GEANT. However, their contribution to the background is negligible [56–58]. The distribution of the intensity of ^{98}Mo

and ^{100}Mo is obtained from a subtraction of the simulated atomic background from the experimental spectra and the uncertainty of this distribution is taken as the square root of the sum of the counts in a considered bin of the experimental spectrum and of the spectrum of the atomic background. The obtained intensity distribution forms a quasicontinuum that contains the intensity of the resolved peaks and the continuum intensity of overlapping weak transitions. The apparent strength in the quasicontinuum is compared with the strength of the resolved peaks in Fig. 11(b). The comparison shows that in the range from 4 MeV to S_n only 20 to 50% of the strength is located in the peaks.

C. Dipole strength deduced from a quasi-continuous spectrum

The quasicontinuum resulting from the subtraction of the atomic background from the experimental spectrum contains the transitions to the ground state (elastic scattering) and in addition, transitions to lower-lying excited states (branching transitions by inelastic scattering) as well as transitions from such states to the ground state (cascade transitions) that cannot be distinguished in our experiments. The first step of the analysis of the quasi-continuum is an estimate of branching and cascade transitions. Cascade simulations were performed by the Monte Carlo procedure described above. Spectra of γ-ray cascades were created for energy bins with a width of $\Delta = 100$ keV. Examples of spectra de-exciting levels from $E_x = 8.2$ to 8.3 MeV in ^{100}Mo are given in the top part of Fig. 13 for three nuclear realizations. As discussed in Sec. II C the maximum energy of an inelastic transition is $E_x - 536$ keV in ^{100}Mo, which is not exactly fulfilled by using a continuous level density instead of the known discrete levels at low energy. However, as can be seen in Fig. 13, the intensity of inelastic transitions in the range from $E_x - 536$ keV to E_x is negligible due to the small level density at low energy (cf. Fig. 9). Starting from the high-energy end of an experimental spectrum, which contains transitions to the ground state only, the simulated intensities of the transitions to the ground state were normalized to the experimental ones in the considered bin and the intensity distribution of the branching transitions was subtracted from the experimental spectrum. Applying this procedure step-by-step for each energy bin moving toward the low-energy end of the spectrum one obtains an intensity distribution that contains transitions to the ground state only. The correction for the branching and cascade transitions is performed for every nuclear realization and a mean distribution of the transitions to the ground state is calculated. This distribution, which is related to the elastic-scattering cross section $\sigma_{\gamma\gamma}$, is compared with the uncorrected quasicontinuum and the distribution resulting from the resolved peaks in the lower part of Fig. 13. As can be seen, the distribution of the ground-state transitions comes close to the distribution of resolved peaks at low energy, whereas it is dominated by the continuum part close to the neutron-separation energy, where the level density is high.

The distribution of the branching ratios B_0 for ^{100}Mo shown in Fig. 14 is simultaneously deduced from the simulations of the γ-ray cascades. The branching ratios B_0 are calculated as

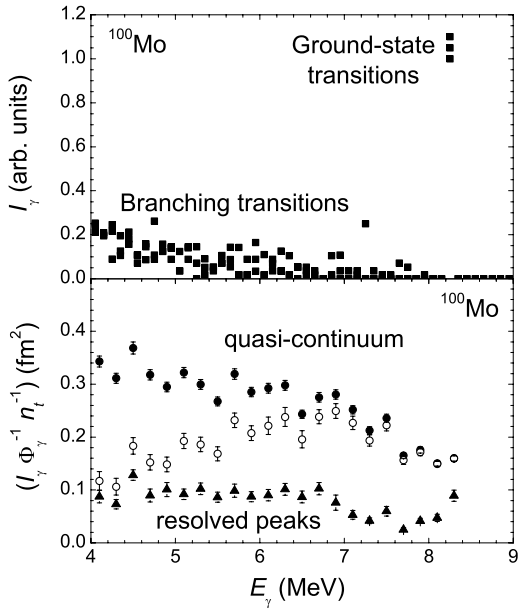

FIG. 13. (Top) Simulated spectra of γ-rays de-exciting levels in ^{100}Mo in the bin from 8.2 to 8.3 MeV for three nuclear realizations. The level scheme of each nuclear realization was built randomly starting from the ground state. (Bottom) Intensity of the quasicontinuum in ^{100}Mo (filled circles) and the remaining intensity distribution of transitions to the ground state after removing the intensities of inelastic transitions (open circles). For comparison, the intensity distribution of the resolved peaks in energy bins of 200 keV is shown with filled triangles. The intensities were corrected for the photon flux Φ_γ and the area density of the target nuclei n_t.

the ratio of the summed intensity $\sum_\Delta I_\gamma^{\text{g.s.}}$ of the transitions to the ground state of the levels in a $\Delta = 100$ keV bin to the summed intensity $\sum_\Delta I_\gamma^{\text{all}}$ of all transitions de-exciting these levels. According to Eqs. (1), (2) we obtain the relation:

$$B_0 = \frac{\sum_\Delta I_\gamma^{\text{g.s}}}{\sum_\Delta I_\gamma^{\text{all}}} = \frac{\sum_{i\,\text{in}\Delta} \Gamma_0^i B_0^i}{\sum_{i\,\text{in}\Delta} \Gamma_0^i}. \tag{15}$$

It can be seen that the values of B_0 for ^{100}Mo are some 60% at low excitation energy where the levels do not have

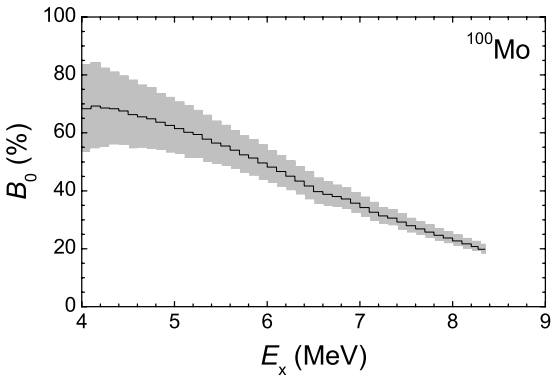

FIG. 14. Distribution of the mean branching ratios B_0 deduced from the cascade simulations for ^{100}Mo averaged over 1000 nuclear realizations. The hatched area shows the 1σ-variation of the mean due to fluctuations of the level spacings and widths.

many possibilities to de-excite to even lower-lying levels. Toward high energy, however, the values of B_0 drop to about 20%, which shows that high-lying levels de-excite via many different branches to lower-lying states. Because of the low level density there is a large scattering of the values of B_0 at energies lower that 4 MeV that makes them useless. Dividing the intensities of the transitions to the ground state, which are proportional to the elastic-scattering cross sections $\sigma_{\gamma\gamma}$, by the corresponding branching ratios B_0 (see Fig. 14), we obtain the absorption cross sections $\sigma_\gamma = \sigma_{\gamma\gamma}/B_0$. The photoabsorption cross sections were obtained by averaging over the values of 1000 nuclear realizations.

The photoabsorption cross sections σ_γ determined in this way are plotted in Fig. 15. They are compared with (γ, n) cross sections [59]. The (γ, n) data were multiplied with a factor of 0.86 according to the findings in Ref. [60]. To show the effect of the reconstruction of the dipole-strength distributions we compare the results for σ_γ with the uncorrected quasicontinuum. The deduced σ_γ are compared with results from ^{98}Mo$(n, \gamma)^{99}$Mo experiments [6] applying Eq. (13). The photoabsorption cross section from experiments with bremsstrahlung at $E_e^{\rm kin} = 3.8$ MeV [25] was calculated for groups of five levels according to Eqs. (12) and (13). Although statistical quantities cannot be derived for a few levels we present the results for σ_γ from the low-lying levels in Fig. 15.

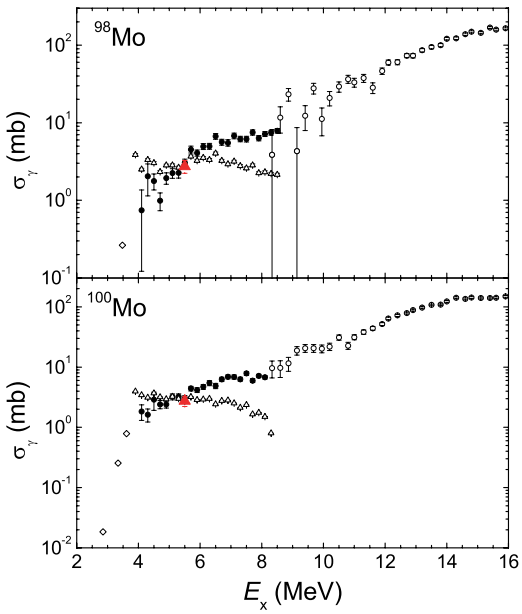

FIG. 15. (Color online) Comparison of the absorption cross section determined from our photon-scattering experiments after correction for feeding and for branching ratios B_0 (filled circles) with those deduced for the (γ, n) reaction [59] (open circles). Open diamonds depict the photoabsorption cross sections from experiments with bremsstrahlung at $E_e^{\rm kin} = 3.8$ MeV. The dipole strength in the neighboring odd-mass ^{99}Mo obtained from (n, γ) experiments [6] is shown as a filled red triangle at 5.5 MeV. The cross section deduced from the intensity of the quasicontinuum without any correction is given with open triangles.

In the following we discuss the influence of the two most important ingredients of the γ-ray cascade simulations, the strength function for $E1$ transitions and the level density, on the results of the analysis. To perform the cascade simulations correctly it is important to achieve a consistency between the input strength function and the deduced photoabsorption cross section at energies below S_n. To test the influence of the strength function for $E1$ transitions on the procedure for the reconstruction we performed simulations for various input strength functions. Examples of the analysis of the ^{100}Mo experiment with various strength functions, a superposition of three Lorentzian curves with energy-dependent widths $[\Gamma(E_x) \sim (E_x)^\delta]$ for $\delta = 1$ as described below and a constant strength function are presented in Fig. 16 in comparison with a parametrization of the GDR by Lorentzians with constant widths ($\delta = 0$). The usage of a constant strength function leads to intense branching transitions and thus to subtraction of large intensity of the quasicontinuum and an under-estimate of the photoabsorption cross section below 6 MeV. The small branching ratios B_0 for transitions from high-lying levels to the ground state of high energy lead to an under-estimate between 6 MeV and S_n. In contrast, the usage of a rapidly increasing strength function based on Lorentzians with $\delta = 1$ leads to

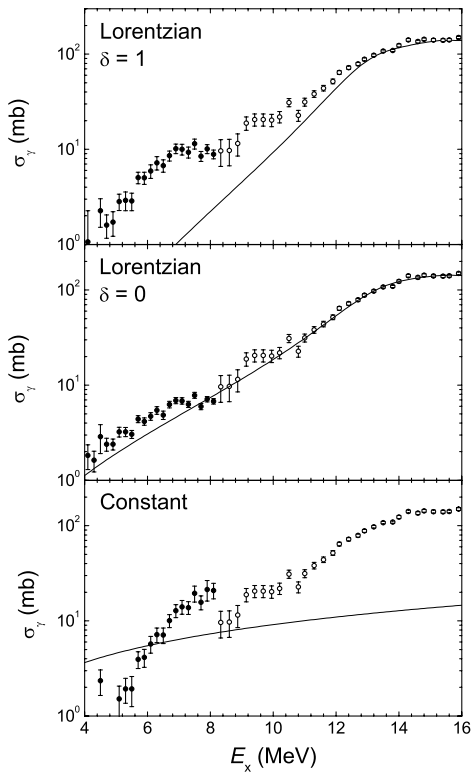

FIG. 16. Analysis of the results of the photon-scattering experiment on ^{100}Mo at $E_e^{\rm kin} = 13.2$ MeV (filled circles) with strength functions (solid lines) from a superposition of three Lorentzian curves with an energy-dependent width ($\delta = 1$, upper panel), with a constant width of ($\delta = 0$, middle panel), and with a constant strength function (bottom panel) included in the simulations of γ-cascades (cf. Sec. IV). The level density was calculated according to the back-shifted Fermi gas model for all cases. The (γ, n) cross sections, taken from Ref. [59], are depicted with open circles.

strong transitions to the ground state and to large ratios B_0 close to S_n. Practically, the $E1$ strength becomes small below 7 MeV and has no strong influence on the reconstruction. The comparison in Fig. 16 shows that the superposition of three Lorentzian curves with constant widths (cf. Sec. IV) gives the best description of the photoabsorption cross section of all presented models at energies above about 5 MeV.

The simulated spectra of γ-ray cascades from levels located at high excitation energies depend strongly also on the model for the level density. The probability for the de-excitation to an intermediate level is related to the number of the levels below the excited one. The two considered models for the level density shown in Fig. 9, the BSFG model and the constant temperature model, predict different densities for the levels in the range around about half of the neutron-separation energy (cf. Fig. 9). This influences the results for the branching ratios B_0 from the γ-ray cascade simulations. We favor the BSFG results because of the convincing agreement of the trend of the data versus the region above the threshold where σ_γ is known [59] as can be seen in Fig. 17. Recent results for the level density in ^{98}Mo from ^{3}He induced experiments [61] support the usage of the BSFG model.

D. Comparison with existing data

The dipole-strength function for ^{98}Mo deduced from the present photon-scattering experiment at $E_e^{\rm kin} = 13.2$ MeV is compared with those obtained from (^{3}He,^{3}He$'\gamma$) experiments and (γ, n) experiments in Fig. 18. In addition the strength in

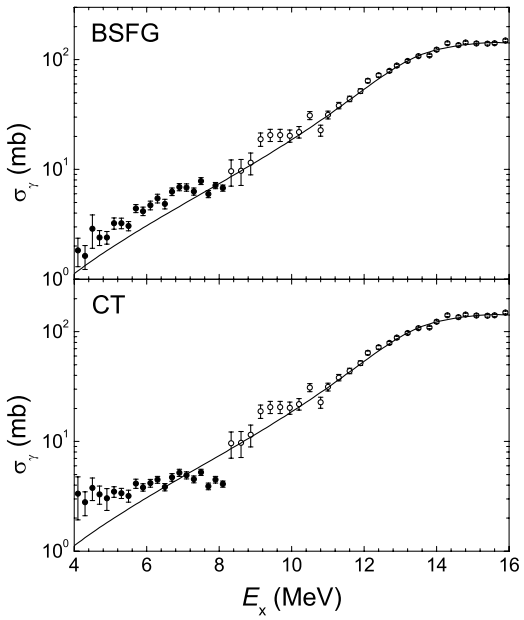

FIG. 17. Analysis of the ^{100}Mo experiment at $E_e^{\rm kin} = 13.2$ MeV (filled circles) with level density calculated according to the BSFG model (upper panel) and to the constant-temperature (CT) model (bottom panel) used in the simulations of γ-ray cascades. A Lorentzian-like strength function (solid line) was used in all simulations. The (γ, n) cross sections taken from Ref. [59] are depicted with open circles.

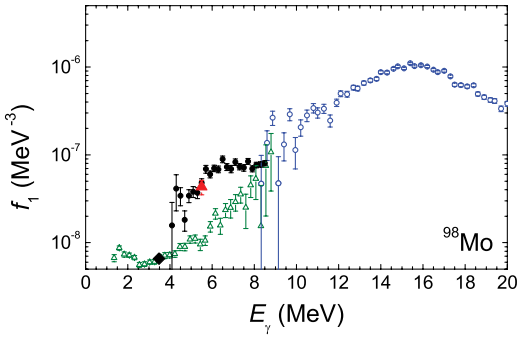

FIG. 18. (Color online) Comparison of the dipole-strength function for ^{98}Mo deduced from the present photon-scattering experiment (black filled circles), from (^{3}He,^{3}He$'\gamma$) experiments [27] (green open triangles), from (n, γ) experiments [6] (red filled triangle at 5.5 MeV), and from (γ, n) experiments [59] (blue open circles). The strength of levels below 4 MeV as taken from Ref. [25] is shown with a filled black diamond at 3.5 MeV.

^{99}Mo deduced from (n, γ) experiments [6] and the strength deduced from our previous photon-scattering experiment at experiment $E_e^{\rm kin} = 4$ MeV [25] are given.

Although the present photon-scattering data agree with the value of the (n, γ) experiment, one observes a disagreement to the data obtained from experiments using the (^{3}He,^{3}He$'\gamma$) reaction [27], especially for the energy dependence of the dipole strength: the slope of the strength versus the energy is nearly by a factor of 2 larger for the results of Ref. [27] than for ours. These data were derived from particle$-\gamma$ coincidences following inelastic scattering of ^{3}He by even-mass Mo targets and by (^{3}He,$\alpha\gamma$) reactions on odd-mass Mo isotopes. These reactions do not deliver an absolute scale for the electromagnetic strength. Therefore, the needed information has to be inferred from (n, γ) data. Differences exist also in the reaction mechanisms. Photons excite mainly $J = 1$ states, whereas ^{3}He ions transfer also higher angular momentum. Due to the large wavelength of the photons their absorption excites the nucleus as a whole and leads to a compound nucleus similarly to the absorption of low-energy neutrons. Consequently one expects an agreement of data obtained by these two methods, which is indeed observed as can be seen in Fig. 15.

IV. PARAMETRIZATION OF THE GDR FOR TRIAXIAL NUCLEI

The chain of stable molybdenum isotopes provides a good example for a study of the dipole strength distributions at the onset of deformation. Because a rigid deformation in the ground state was observed in the heavier ^{104}Mo and ^{106}Mo isotopes [62] and the lightest ^{92}Mo is a closed-shell nucleus, the intermediate isotopes ^{98}Mo and ^{100}Mo are expected to show characteristics of transitional nuclei. The shapes of ^{98}Mo [63] and ^{96,100}Mo [64] were recently investigated by means of Coulomb-excitation experiments. It was found that the quadrupole deformations of ^{98}Mo and ^{100}Mo are $\beta_2 = 0.19(5)$ and $\beta_2 = 0.24(5)$, respectively. The experimentally deduced shapes of the considered Mo isotopes are soft where the

triaxiality parameter γ for ^{98}Mo is 32° [63]. Therefore, the properties of the investigated Mo isotopes are influenced by the quadrupole deformation and the triaxial shape.

According to the hydrodynamical model the GDR is represented as a vibration of the proton system against the neutron system. The GDR may be reproduced by a Lorentzian curve. For nuclei with stable deformation in the ground state, the GDR is considered as a superposition of independent vibrations along every principal axis of the nucleus such that the strength conserves. The integrated photoabsorption cross section is given by the Thomas-Reiche-Kuhn dipole-sum rule $\int \sigma_\gamma(E_x)dE_x = 60ZN/A$ mb MeV [65]. For the triaxially deformed nuclei the GDR splits into three peaks with energies inversely proportional to the length of the semiaxis. According to Ref. [66] the energies of the maxima $E_i (i = 0, 1, 2)$ of each peak are given by:

$$E_i = E_0 \exp\left[-\sqrt{\frac{5}{4\pi}}\beta_2 \cos\left(\gamma - \frac{2}{3}\pi i\right)\right], \qquad (16)$$

where E_0 is the GDR energy of a spherical nucleus. The Hill-Wheeler parameters β_2 and γ used in Eq. (16) were taken from Ref. [25].

A stable deformation of the ground state results in a rotational motion with an energy of about two orders of magnitude smaller than E_0. Thus, the GDR vibration is decoupled from rotation. Low-spin excitations like surface vibrations may differ from the GDR energy E_0 by a factor of 10 such that in spite of a quasiadiabatic approximation the coupling of the two motions leads to satellites of the GDR appearing at higher energies. The number of observable satellites depends on the strength of the low-energy vibration, but in any case they will not change the low-energy slope of the GDR.

We attempt to parametrize the low-energy tail of the GDR by a Lorentzian. As was shown theoretically [4] a description of the photoabsorption cross section by a Lorentzian is appropriate albeit the total width Γ of a GDR in a heavy nucleus is dominated by spreading [59,67] and not by escape, i.e., direct decay. Considering the wide range of excitation energy spanned by the combined data, a test of a Lorentzian with energy-dependent total width $\Gamma(E_x)$ is indicated:

$$\sigma_\gamma(E_x) = \frac{2C \times S_{\mathrm{TRK}}}{3\pi} \sum_{i=1}^{3} \frac{E_x^2 \Gamma(E_x)}{\left(E_i^2 - E_x^2\right)^2 + E_x^2 \Gamma(E_x)^2}. \qquad (17)$$

The parameter C measures the conformance of the integrated $E1$ strength with the Thomas-Reiche-Kuhn sum rule. We use the parametrization $\Gamma(E_x) = \Gamma_S \times (E_x/E_i)^\delta$ of the energy dependence of the width [66], with δ as a parameter to be defined by a fit to the combined data.

The coupling of the particle-hole states constituting the main component of the GDR to more complicated configurations results in a Lorentzian shape [4] with a width determined by the size of this coupling, which acts like a damping. From fits to GDR of different peak energy (in nuclei with different mass number A) a proportionality between damping width and energy was found [5] but also a dependence of damping width on the excitation energy stronger than linear was reported [66,68]. Because of their limited range and accuracy, data within single nuclei did not allow a precise determination of the energy dependence of the damping width. A parametrization of the GDR including energy dependence of the damping width, i.e. $\delta = 1$, is shown in Fig. 19. The most accurate (n, γ) data published so far [69] indicate a rather weak increase of the $E1$ strength with the excitation energy in ^{108}Ag.

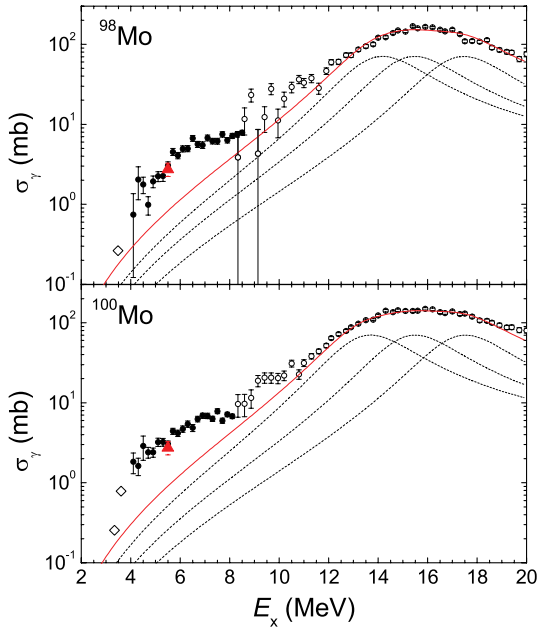

FIG. 19. (Color online) Comparison of determined photoabsorption cross section from the photon-scattering experiments on ^{98}Mo and ^{100}Mo at $E_e^{\mathrm{kin}} = 13.2$ MeV (filled circles) and the measured cross section for (γ, n) reaction [59] (open circles) with the parametrization of the GDR (red solid line) for $\delta = 1$ [see Eq. (17)]. The GDR is represented as a superposition of three Lorentzians corresponding to the triaxial shape of the nuclei (dotted lines). The photoabsorption cross section deduced from the levels below 4 MeV [25] is shown with open diamonds. The cross section for ^{99}Mo calculated from the strength function deduced from (n, γ) measurements [6] is depicted with a filled red triangle at 5.5 MeV.

From the slopes below the resonance energy we obtain $\delta = 0.0(4)$, i.e., no energy dependence of the width within the uncertainty. In accordance to our findings in the neighboring nucleus ^{88}Sr [35] and to the systematics of the GDR widths [68] we use $\Gamma_S = 4$ MeV. For the parameter C we find values of 0.92(13), 0.90(13) from fits of (γ, n) data of ^{98}Mo and ^{98,100}Mo, respectively. The results of the parametrization are presented in Fig. 20. One observes some extra strength with respect to the parametrization of the GDR by a Lorentzian in the energy range from about 4 to about 8 MeV. This extra strength amounts to about 0.3% of the Thomas-Reiche-Kuhn sum rule.

By using the proposed separation of the two reasons for the widening of the GDR (deformation and spreading), we obtain an expression of use also when no GDR data are available, which is of importance for nuclei far off stability entering nucleosynthesis calculations. Without much influence on the off-resonance cross section the GDR energy can then be taken from systematics [70] in combination with $C = 1$ and with calculated deformation parameters [25], resulting in

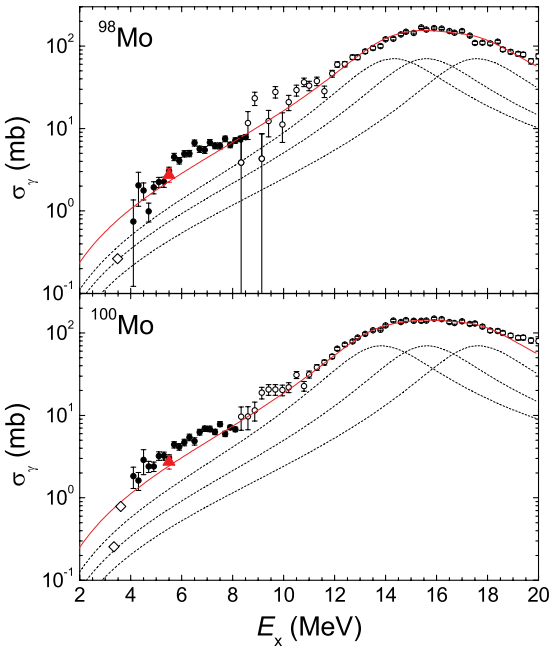

FIG. 20. (Color online) The same as described in the caption to Fig. 19 but for parameter $\delta = 0$.

predictions for the dipole strength from about 5 MeV up to the neutron-separation energies.

V. SUMMARY

The response of ^{98}Mo and ^{100}Mo to dipole radiation was investigated at the bremsstrahlung facility at the superconducting linear electron accelerator ELBE of the Forschungszentrum Dresden-Rossendorf. The photon-scattering experiments were carried out at an electron-beam energy higher than the neutron-separation energies of the Mo isotopes that allowed us to study the dipole strength close to the threshold for the (γ, n) reaction at a high photon flux. The number of transitions assigned to ^{98}Mo and ^{100}Mo is 485 and 499, respectively, the main part of them being dipole transitions.

Because of the Porter-Thomas fluctuations of the level widths most of the levels do not appear as resolved peaks in the experimental spectra. Instead, weakly populated levels produce a quasicontinuum of overlapping peaks due to the high level density above 5 MeV and the finite resolution of the detectors. A comparison of the spectra of ^{98}Mo and ^{100}Mo shows that close to the neutron-separation energy of ^{98}Mo the strength in the quasicontinuum is two times higher than the strength in the peaks. GEANT3 simulations were applied to determine the background due to atomic processes in the measured spectra and thus to extract the quasicontinuum. The continuum contains the elastic transitions to the ground state as well as the inelastic transitions to low-lying levels as well as the cascade transitions subsequently de-excitating these levels.

A Monte Carlo code for simulations of γ-ray cascades was developed that allows us (i) to deconvolute the intensity distribution of the transitions to the ground state from the quasicontinuum and thus to determine the cross section for elastic scattering and (ii) to calculate the branching ratios for transitions to the ground state and to obtain the photoabsorption cross section. Because the obtained photoabsorption cross sections for ^{98}Mo and ^{100}Mo match the measured cross sections for the (γ, n) reaction this method allows us to determine the tail of the GDR below the neutron-separation energy. To test the results of the simulations experimentally, in particular the calculated branching ratios, we plan an experiment with a monoenergetic photon beam at the HIγS facility of Duke University.

We parametrized the GDR as a superposition of three Lorentzian curves with maxima depending on the stable ground-state deformations along the three principal axes of a triaxially deformed nucleus. The experimental data are compatible with Lorentzians of an energy-independent width.

Note added in proof. A possible difference between the absolute scale for the dipole strength of ^{96}Mo, as published in a recent paper by Krtička *et al.* in Phys. Rev. C **77**, 054319 (2008), and the scale for the ^{98,100}Mo isotopes according to the present article needs further investigation. It is to be noted that the normalization of the dipole strength used by Krtička *et al.* relied on a correct reproduction of the average radiation width of several *s*-wave resonances in the system ^{95}Mo+n, whereas in the present work the dipole strength is delivered in absolute units directly by the method itself.

ACKNOWLEDGMENTS

We thank P. Michel and the ELBE-Crew, who made these experiments possible with their strong commitment to deliver optimum beams. Thanks are due to A. Hartmann and W. Schulze for their valuable support during the difficult experiments. Helpful discussions with S. Frauendorf and R. Wünsch are gratefully acknowledged. This work was supported by the Deutsche Forschungsgemeinschaft under contract DO-466/1-2. F.B. and M.K. acknowledge the support by the Ministry of Education of the Czech Republic under contract MSM0021620859.

[1] M. Goldhaber and E. Teller, Phys. Rev. **74**, 1046 (1948).
[2] H. Steinwedel and J. Jensen, Z. Naturforschung **5a**, 413 (1950).
[3] W. D. Myers, W. J. Swiatecki, T. Kodama, L. J. El-Jaick, and E. R. Hilf, Phys. Rev. C **15**, 2032 (1977).
[4] C. B. Dover, R. H. Lemmer, and F. J. W. Hahne, Ann. Phys. (NY) **70**, 458 (1972).
[5] J. Wambach, Rep. Prog. Phys. **51**, 989 (1988).
[6] J. Kopecky and M. Uhl, *Proceedings of the NEA/ENEA and IAEA Specialists' Meeting on Measurement, Calculation and Evaluation of Photon Production Data*, Bologna, November 9-17, 1994.
[7] S. G. Kadmenskii, V. P. Markushev, and V. I. Furman, Soviet J. Nucl. Phys. **37**, 165 (1983).
[8] P. Axel, Phys. Rev. **126**, 671 (1962).
[9] R. M. Laszewski and P. Axel, Phys. Rev. C **19**, 342 (1979).

[10] R. Alarcon, R. M. Laszewski, A. M. Nathan, and S. D. Hoblit, Phys. Rev. C **36**, 954 (1987).
[11] G. A. Bartholomew, E. D. Earle, A. J. Ferguson, J. W. Knowles, and M. A. Lone, Adv. Nucl. Phys. **7**, 229 (1973).
[12] U. Kneissl, N. Pietralla, and A. Zilges, J. Phys. G: Nucl. Part. Phys. **32**, R217 (2006).
[13] N. Ryezayeva, T. Hartmann, Y. Kalmykov, H. Lenske, P. von Neumann-Cosel, V. Yu. Ponomarev, A. Richter, A. Shevchenko, S. Volz, and J. Wambach, Phys. Rev. Lett. **89**, 272502 (2002).
[14] E. Litvinova, P. Ring, and D. Vretenar, Phys. Lett. **B647**, 111 (2007).
[15] N. Tsoneva and H. Lenske, J. Phys. G: Nucl. Part. Phys. **35**, 014047 (2008).
[16] B. L. Berman and S. C. Fultz, Rev. Mod. Phys. **47**, 713 (1975).
[17] S. Goko, H. Utsunomiya, S. Goriely, A. Makinaga, T. Kaihori, S. Hohara, H. Akimune, T. Yamagata, Y.-W. Lui, H. Toyokawa, A. J. Koning, and S. Hilaire, Phys. Rev. Lett. **96**, 192501 (2006).
[18] F. R. Metzger, Prog. Nucl. Phys. **7**, 53 (1959).
[19] U. Kneissl, H. H. Pitz, and A. Zilges, Prog. Part. Nucl. Phys. **37**, 349 (1996).
[20] K. S. Krane, At. Data Nucl. Data Tables **16**, 383 (1975).
[21] W. D. Hamilton, edited by, *The Electromagnetic Interaction in Nuclear Spectroscopy* (North-Holland, Amsterdam, 1975).
[22] S. Goriely, Phys. Lett. **B436**, 10 (1998).
[23] E. M. Burbridge, G. R. Burbridge, W. A. Fowler, and F. Hoyle, Rev. Mod. Phys. **29**, 547 (1957).
[24] S. Goriely and E. Khan, Nucl. Phys. **A706**, 217 (2002).
[25] G. Rusev, R. Schwengner, F. Dönau, M. Erhard, S. Frauendorf, E. Grosse, A. R. Junghans, L. Käubler, K. Kosev, L. K. Kostov, S. Mallion, K. D. Schilling, A. Wagner, H. von Garrel, U. Kneissl, C. Kohstall, M. Kreutz, H. H. Pitz, M. Scheck, F. Stedile, P. von Brentano, C. Fransen, J. Jolie, A. Linnemann, N. Pietralla, and V. Werner, Phys. Rev. C **73**, 044308 (2006).
[26] Z. Szefliński, G. Szeflińska, Z. Wilhelmi, T. Rzaca-Urban, H. V. Klapdor, E. Anderson, K. Grotz, and J. Metzinger, Phys. Lett. **B126**, 159 (1983).
[27] M. Guttormsen, R. Chankova, U. Agvaanluvsan, E. Algin, L. A. Bernstein, F. Ingebretsen, T. Lönnroth, S. Messelt, G. E. Mitchell, J. Rekstad, A. Schiller, S. Siem, A. C. Sunde, A. Voinov, and S. Ødegård, Phys. Rev. C **71**, 044307 (2005).
[28] J. Kopecky and M. Uhl, Phys. Rev. C **41**, 1941 (1990).
[29] T. J. Bowles, R. J. Holt, H. E. Jackson, R. M. Laszewski, R. D. McKeown, A. M. Nathan, and J. R. Specht, Phys. Rev. C **24**, 1940 (1981).
[30] G. Rusev, PhD dissertation, Technische Universität Dresden, 2007 (Wissenschaftlich-Technische Berichte, FZD-478, 2007); https://www.fzd.de/publications/010008/10008.pdf.
[31] F. Bĕcvář, Nucl. Instrum. Methods A **417**, 434 (1998).
[32] T. von Egidy and D. Bucurescu, Phys. Rev. C **72**, 044311 (2005).
[33] Y. Kalmykov, T. Adachi, G. P. A. Berg, H. Fujita, K. Fujita, Y. Fujita, K. Hatanaka, J. Kamiya, K. Nakanishi, P. von Neumann-Cosel, V. Yu. Ponomarev, A. Richter, N. Sakamoto, Y. Sakemi, A. Shevchenko, Y. Shimbara, Y. Shimizu, F. D. Smit, T. Wakasa, J. Wambach, and M. Yosoi, Phys. Rev. Lett. **96**, 012502 (2006).
[34] T. A. Brody, J. Flores, J. B. French, P. A. Mello, A. Pandey, and S. S. M. Wong, Rev. Mod. Phys. **53**, 385 (1981).
[35] R. Schwengner, G. Rusev, N. Benouaret, R. Beyer, M. Erhard, E. Grosse, A. R. Junghans, J. Klug, K. Kosev, L. Kostov, C. Nair, N. Nankov, K. D. Schilling, and A. Wagner, Phys. Rev. C **76**, 034321 (2007).
[36] N. Pietralla, Z. Berant, V. N. Litvinenko, S. Hartman, F. F. Mikhailov, I. V. Pinayev, G. Swift, M. W. Ahmed, J. H. Kelley, S. O. Nelson, R. Prior, K. Sabourov, A. P. Tonchev, and H. R. Weller, Phys. Rev. Lett. **88**, 012502 (2001).
[37] F. Bĕcvář, P. Cejnar, J. Honzátko, K. Konečný, I. Tomandl, and R. E. Chrien, Phys. Rev. C **52**, 1278 (1995).
[38] M. Krtička, F. Bĕcvář, J. Honzátko, I. Tomandl, M. Heil, F. Käppeler, R. Reifarth, F. Voss, and K. Wisshak, Phys. Rev. Lett. **92**, 172501 (2004).
[39] http://www-nds.iaea.org/RIPL-2/.
[40] C. E. Porter and R. G. Thomas, Phys. Rev. **104**, 483 (1956).
[41] R. Schwengner, R. Beyer, F. Dönau, E. Grosse, A. Hartmann, A. R. Junghans, S. Mallion, G. Rusev, K. D. Schilling, W. Schulze, and A. Wagner, Nucl. Instrum. Methods A **555**, 211 (2005).
[42] A. Wagner, R. Beyer, M. Erhard, F. Dönau, E. Grosse, A. Hartmann, A. R. Junghans, L. Käubler, K. Kosev, S. Mallion, C. Nair, N. Nankov, G. Rusev, K. D. Schilling, W. Schulze, and R. Schwengner, J. Phys. (London) G **31**, S1969 (2005).
[43] CERN Program Library Long Writeup W5013, Geneva 1993, unpublished.
[44] F. Ajzenberg-Selove, Nucl. Phys. **A506**, 1 (1990).
[45] D. R. Tilley, H. R. Weller, and C. M. Cheves, Nucl. Phys. **A564**, 1 (1993).
[46] U. E. P. Berg, K. Ackermann, K. Bangert, C. Bläsing, W. Naatz, R. Stock, K. Wienhard, M. K. Brussel, T. E. Chapuran, and B. H. Wildenthal, Phys. Lett. **B140**, 191 (1984).
[47] G. Roche, C. Ducos, and J. Proriol, Phys. Rev. A **5**, 2403 (1972).
[48] E. Haug, Radiat. Phys. Chem. **77**, 207 (2008).
[49] K. Vogt, P. Mohr, M. Babilon, J. Enders, T. Hartmann, C. Hutter, T. Rauscher, S. Volz, and A. Zilges, Phys. Rev. C **63**, 055802 (2001).
[50] R. A. I. Bell, R. D. Gill, B. C. Robertson, J. S. Lopes, and H. J. Rose, Nucl. Phys. **A118**, 481 (1968).
[51] M. N. H. Comsan, M. A. Farouk, A. A. El-Kamhawy, M. S. M. El-Tahawy, and A. N. Lvov, Z. Phys. **212**, 71 (1968).
[52] A. Artna-Cohen, Nucl. Data Sheets **70**, 85 (1993).
[53] L. K. Peker, Nucl. Data Sheets **73**, 1 (1994).
[54] R. Jenkins, R. W. Gould, and D. Gedke, *Quantitative X-Ray Spectroscopy* (Dekker, New York, 1995).
[55] A. A. Al-Beteri and D. E. Raeside, Nucl. Instrum. Methods B **44**, 149 (1989).
[56] Z. Berant, R. Moreh, and S. Kahane, Phys. Lett. **B69**, 281 (1977).
[57] M. Schumacher, F. Smend, W. Mückenheim, P. Rullhusen, and H. G. Börner, Z. Phys. A **300**, 193 (1981).
[58] H. Falkenberg, A. Hünger, P. Rullhusen, M. Schumacher, A. I. Milstein, and K. Mork, At. Data Nucl. Data Tables **50**, 1 (1992).
[59] H. Beil, R. Bergère, P. Carlos, A. Leprêtre, A. De Miniac, and A. Veyssière, Nucl. Phys. **A227**, 427 (1974).
[60] B. L. Berman, R. E. Pywell, S. S. Dietrich, M. N. Thompson, K. G. McNeill, and J. W. Jury, Phys. Rev. C **36**, 1286 (1987).
[61] R. Chankova, A. Schiller, U. Agvaanluvsan, E. Algin, L. A. Bernstein, M. Guttormsen, F. Ingebretsen, T. Lönnroth, S. Messelt, G. E. Mitchell, J. Rekstad, S. Siem, A. C. Larsen, A. Voinov, and S. Ødegård, Phys. Rev. C **73**, 034311 (2006).
[62] E. Cheifetz, R. C. Jared, S. G. Thompson, and J. B. Wijhelmy, Phys. Rev. Lett. **25**, 38 (1970).

[63] M. Zielińska, T. Czosnyka, J. Choiński, J. Iwanicki, P. Napiorkowski, J. Srebrny, Y. Toh, M. Oshima, A. Osa, Y. Utsuno, Y. Hatsukawa, J. Katakura, M. Koizumi, M. Matsuda, T. Shizuma, M. Sugawara, T. Morikawa, H. Kusakari, A. D. Efimov, and V. M. Mikhajlov, Nucl. Phys. **A712**, 3 (2002).

[64] K. Wrzosek, M. Zielińska, J. Choiński, T. Czosnyka, Y. Hatsukawa, J. Iwanicki, J. Katakura, M. Kisieliński, M. Koizumi, M. Kowalczyk, H. Kusakari, M. Matsuda, T. Morikawa, P. Napiorkowski, A. Osa, M. Oshima, L. Reissig, T. Shizuma, J. Srebrny, M. Sugawara, Y. Toh, Y. Utsuno, and K. Zajac, Int. J. Mod. Phys. E **15**, 374 (2006).

[65] S. S. Dietrich and B. L. Berman, At. Data Nucl. Data Tables **38**, 199 (1988).

[66] B. Bush and Y. Alhassid, Nucl. Phys. **A531**, 27 (1991).

[67] G. F. Bertsch, Nature **280**, 639 (1979).

[68] P. Carlos, R. Bergère, H. Beil, A. Leprêtre, and A. Veyssière, Nucl. Phys. **A219**, 61 (1974).

[69] L. Zanini, F. Corvi, H. Postma, F. Bečvář, M. Krtička, J. Honzátko, and I. Tomandl, Phys. Rev. C **68**, 014320 (2003).

[70] A. Bohr and B. Mottelson, *Nuclear Structure* (W. A. Benjamin, Amsterdam, 1975), Chapt. 6.